

Copolymerizing Lignin for Tuned Properties of 3D-Printed PEG-Based Photopolymers

Ana Laura Ruiz Deance, Bjorn Siersema, Laurine Eleonora Anne-Catherine Yoe, Frederik R. Wurm, and Hubert Gojzewski*



Cite This: *ACS Appl. Polym. Mater.* 2023, 5, 10021–10031



Read Online

ACCESS |



Metrics & More



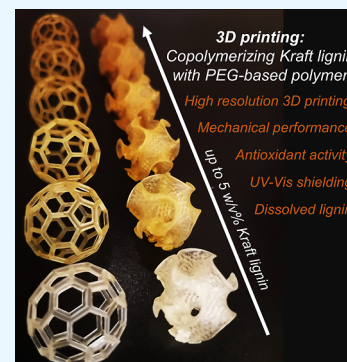
Article Recommendations



Supporting Information

ABSTRACT: The global emphasis on environmental conservation has sparked the exploration for alternative materials to replace nonrenewable petroleum-based products. With abundant lignocellulosic biomass, there is a growing focus on designing biobased polymers with enhanced properties. In this work, we prepared lignin-containing copolymer macrostructures by 3D printing of poly(ethylene glycol) diacrylate (PEGDA) and biobased methacrylated Kraft lignin. Studied lignin loading is up to 10 w/v %. Liquid crystal display stereolithography was used to 3D print models of varying complexities and sizes. We demonstrate that methacrylated lignin can be thoroughly dissolved within the polyPEGDA matrix. This enables the adjustment of light shielding, mechanical performance, and antioxidant activity in the final high-resolution 3D-printed materials. Adding just 1 w/v % of the lignin-based component to the translucent (visible light) and brittle polyPEGDA reduces the transmittance of visible light to only 30% (at 550 nm). Additionally, it improves the elongation at break by a factor of 1.5 when compared with pure PEGDA-based resins. Moreover, the antioxidant properties of lignin further enhance the materials, resulting in approximately 40% antioxidant activity. The 3D-printed materials under study can then be considered as structures that block light and inhibit oxygen, making them suitable for applications in biotechnology.

KEYWORDS: 3D printing, PEGDA, lignin, photopolymerization, light shielding, elasticity, antioxidant activities



1. INTRODUCTION

Due to growing societal demand for sustainable materials, various biopolymers have received significant attention in recent years.¹ One particular focus is the utilization of lignin, which is the second most abundant biopolymer, accounting for $\approx 30\%$ of organic carbon in the biosphere.^{2–4} Beyond its renewable and biodegradable nature, lignin's high thermal stability, chemical resistance, rigid structure, antioxidant properties, and functionalizability make it an excellent option for biobased polymers or additives.^{1,2,5–7} Some of the physicochemical properties can already be controlled at the lignin's processing methods by the Kraft or Organosolv processes or as lignosulfonates.^{8,9}

For instance, recently, both the pavement engineering and tire industries have recognized the value of lignin as a component in asphalt and rubber, serving as coupling agents, emulsifiers, and fillers.^{10–13} The properties of lignin have also been considered a valuable additive in polymeric materials, particularly in blends or composites.¹⁴ Of note are polymer-based products that have been introduced on the market, constructed using lignin, i.e., headphones (TECNARO GMBH, model AudioQuest Nighthawk). Also, lignin and its derivatives hold promise for applications in the pharmaceutical and cosmetic sectors as well as medicine or agriculture.^{15–17} They have the potential to be excipients in drugs and skincare products, offering benefits like antioxidants and UV radiation

absorption.^{18–20} There are also fascinating works that argue that lignin can serve as a drug and gene delivery vehicle.^{21–23}

However, only a few reports utilized lignin in 3D printing due to its low solubility or incompatibility with the matrix.^{4,24} 3D printing (additive manufacturing) is an automated fabrication process of creating three-dimensional objects by adding material layer-by-layer.²⁵ It enables the production of custom objects from digital designs, eliminating traditional subtractive methods such as cutting, masking, or molding. This technology finds extensive applications in industry, research, and daily life for creating three-dimensional structures from materials such as metals, ceramics, and polymers.²⁶ For the latter, the use of biobased polymers as matrices and additives is highly attractive.

As 3D printing is continuously being researched and developed, many methods are available to 3D print using biopolymers, like lignin. These are primarily fused filament fabrication (FFF), direct ink writing (DIW), and stereolithography (SLA).^{4,24–26} By combining lignin's abundance

Received: August 15, 2023
Revised: October 26, 2023
Accepted: October 26, 2023
Published: November 7, 2023

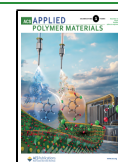


Table 1. Lignin Components in Polymer Materials 3D-Printed Using SLA and Consequent Technologies

lignin type	lignin loading	lignin physicochemical form in matrix	matrix chemically known	matrix and filler mixing	final material	comments	refs
Kraft	0.2–1.0 wt %	particles; sizes: nm to μm	no	dispersion	composite	improved mechanical performance only when postcured	28
Organosolv	5–15 wt %	macromolecule	no	dissolution	copolymer	ductile specimens	32
lignin-coated cellulose nanocrystals	0.1–1.0 wt %	unknown	no	dispersion	composite	thermal stability improved	33,34
soda	26–39 wt %	macromolecule	yes	dissolution	polymer	printability required heated resin (40°C)	35
Kraft	0.5–2.0 wt %	nanoparticles; ca. 100 nm	yes	dispersion	nanocomposite	biobased resin used	29
dealkaline-lignin	2.5 wt %	particles; sizes: μm	yes	dispersion	composite/blend	hindered dispersion	30
dealkaline-lignin	1.0 wt %	particles; sizes: nm to μm	yes	dispersion	composite	lignin as photoinitiator	31
Organosolv	5.0 wt %	unknown	no	unknown	unknown	critical cure dosage compared	36

and renewability with its customizable physicochemical processing and diverse 3D-printing methods mentioned earlier, lignin offers a platform for innovative materials with unconventional functionalities, reducing the need for fossil-derived polymers. Designing the starting material appropriately is not straightforward as the addition of lignin affects various conditions in 3D printing, such as melt rheology in FFF, viscoelasticity in DIW, or light-curing ability in SLA.⁴ Furthermore, when used as a pure filler, lignin typically weakens the overall performance of the final material, necessitating chemical modification for proper dispersion within the polymer matrix.^{4,27} This issue is especially pronounced in vat photopolymer 3D printing, including SLA and related technologies, as unmodified lignin struggles to achieve homogeneous dispersion and solubility in liquid epoxy- or (meth)acrylate-based resins.^{28–31} This leads to phase separation or sedimentation during printing, resulting in structural inhomogeneity in the final material.

In 2019, Zhang et al. reported the use of Kraft lignin for SLA that led to improved mechanical properties of samples already at a small lignin loading of only 0.4 wt %.²⁸ However, the unmodified lignin remained insoluble in the matrix, resulting in the formation of composites with particles ranging from tens of nm to tens of μm . This variance hindered layer uniformity and limited its thickness (maximum 100 μm). Additionally, operable lignin content needed to be <1 wt %. Above this threshold, samples experienced darkening and mechanical softening, likely attributed to the lignin particles strongly competing with the photoinitiator in the resin's cross-linking process.²⁰ Similarly, Sutton et al. have used Organosolv lignin for 3D printing by SLA.³² The authors acrylated the lignin and dissolved it in a commercial resin PR48 (Autodesk/Colorado Photopolymer Solutions), which is composed of 3 different acrylates, and reported improved ductility of the printed samples. Samples containing a high lignin content (up to 15 wt %) in the matrix were 3D-printed. This was possible because Organosolv lignin exhibits lower UV absorption (thus less competitive to the photoinitiator) and lower molar mass (thus boosting 3D printing as compositions were moderately viscous) compared to Kraft lignin.²⁰ More complex systems were proposed, for instance, by Feng et al. with lignin-coated cellulose nanocrystals incorporated into methacrylate resin.³³ Samples with these fillers exhibited a higher storage modulus in the rubbery plateau; however, micrometer-sized aggregates were formed during the dispersion of the nanocrystals in the

matrix. In Table 1, we provide a summary of the current literature on the use of lignin in polymer materials 3D-printed using SLA and consequent technologies. As can be evidenced, the maximum Kraft lignin loading in a resin reported is 2 wt %, which is also not molecularly dissolved but dispersed.

In this work, we used liquid crystal display (LCD) SLA 3D printing for the statistical copolymerization of the methacrylated Kraft lignin with poly(ethylene glycol) diacrylate (PEGDA). Unlike resins, which were previously combined with lignin,^{28,32,33,37} PEGDA is of a known chemical structure and is commonly used in various biomedical applications.^{38,39} For example, PEGDA-based materials are well-tolerated by living organisms (biocompatibility), show adaptability to specific application requirements (tunable), are advantageous for use in aqueous environments (water-solubility or swelling), and possess the ability to encapsulate drugs within the hydrogel network. PEGDA has also been noted as an excellent material for 3D printing; however, it has the following drawbacks: poor UV/vis-shielding, limited mechanical performance (especially brittleness), and is of a fossil origin (a fully synthetic polymer).^{40–42} By the incorporation of the copolymerizing lignin component in PEGDA, we show that these drawbacks can be reduced. We demonstrate that our resin, with its high-quality 3D printability, can serve as a platform that combines the biomedical capabilities of PEGDA and lignin, resulting in a final material with enhanced properties.

2. EXPERIMENTAL SECTION

2.1. Methacrylation of Kraft Lignin. Lignin was modified by esterification with methacrylic anhydride following a previously reported procedure.²² In brief, 10 g of Kraft lignin (Lineo Classic G, Stora Enso, Finland) was dissolved in 150 mL of dimethylformamide (DMF) with lithium chloride (3.5 g) at 90 °C under argon. After complete dissolution, the temperature was reduced to 50 °C, and 5 mL of triethylamine (10 mmol) was added to the solution and stirred for 15 min. Thereafter, 15 mL of methacrylic anhydride (20 mmol) was added dropwise into the reaction mixture, and the reaction was maintained at 50 °C overnight. The crude mixture was precipitated into ca. 1 L of isopropanol and obtained as a brown to black powder. The product was again dissolved in chloroform and precipitated again into 2-propanol, filtered, and washed again with isopropanol. Finally, the product was dried at room temperature in a vacuum oven to yield the methacrylated Kraft lignin in typical yields of approximately 80%.

2.2. Formulation Preparation. The oligomeric resin poly(ethylene glycol) diacrylate (PEGDA, $M_n = 575 \text{ g mol}^{-1}$, Merck) was stirred with a magnetic stirrer at 500 rpm with a diphenyl-(2,4,5-trimethylbenzoyl) phosphine oxide (TPO, >98%, Tokyo Chemical Industry) photoinitiator at 2 w/v % for 2 h at room temperature, prior to the addition of the methacrylated lignin. Thereafter, eight mixtures at 80–100 mL, containing 0, 0.5, 1.0, 2.0, 3.0, 5.0, 7.5, and 10 w/v % (to the volume of PEGDA) of the methacrylated lignin, were prepared using a shaker (Knytel, model K-MI0103002) for 12–24 h at 250 rpm in flasks covered with aluminum foil. Examples of compositions are shown in the Supporting Information (Figure S1). The prepared mixtures were used for 3D printing.

2.3. 3D Printing and Settings. The lignin-containing resin mixtures were 3D-printed in a bottom-up configuration using a Zortrax Inkspire 3D printer at room temperature. This 3D printer utilizes a 405 nm LED source (single lamp) controlled by an LCD screen to cure resins layer-by-layer in a vat with a tray made of fluorinated ethylene propylene (FEP) foil. Z-Suite Zortrax software version 2.30 was utilized for slicing, programming settings, and printing various models, including tensile bars (ASTM-D638, type IV), as well as models with varying degrees of complexity, such as an elephant, nanotube, fullerene, gyroid sphere, and a logo. The programmed layer thickness was set to 50 μm per layer. For tensile bars, the printing direction was aligned with the longest dimension. It was done to evaluate their mechanical properties with the applied forces and bulk interfaces in an orthogonal configuration.

The viscosity of the resins judged by the naked eye did not vary significantly, so the platform speed for the vertical movement was set to a constant value of 75 mm min^{-1} (withdraw and approach). The lift of the platform was set to 3 mm.

To determine the appropriate UV irradiation dosage for each printed layer, the “exposure time calibration” (ETC) tool was used in the 3D printer’s software. This tool eliminated the need for establishing Jacob’s working curve, which relates the absorbed UV light energy to the cured thickness of a photopolymer during UV light exposure.⁴³ Utilizing the ETC tool, we printed a model sample consisting of 10 columns, each having identical features. These columns were subjected to varying UV irradiation times. This test unveiled distinct curing efficiencies within specific columns, encompassing features that were either not cured, undercured, well-cured, or overcured (Figure S2 in the Supporting Information). Through visual inspection, we determined the minimum irradiation time required to achieve accurate printing and produce a stable object for the features within a column. To enhance the precision of our selection, we initially employed a broad range for the search irradiation time, such as increasing it by 5 s for each successive column. Once the range of irradiation time at which the material shows curing evidence was known, we narrowed the irradiation time search with increments of 1 s between columns to finally select the desired irradiation time. In our case, the irradiation time was determined to be 11 and 40 s for PEGDA and lignin-based samples, respectively. The irradiation time of each bottom layer in the columns (the layers located underneath the printed structure, whose task is to achieve adhesive stabilization of the printed model with the platform) was set to 120 s. The excess of the photopolymer on the printed objects (uncured, sticked resin) was removed by a 1 min ultrasonication bath in a mixture of water and isopropanol (50:50 vol %).

2.4. Characterization Methods. **2.4.1. ³¹P NMR Spectroscopy.** ³¹P nuclear magnetic resonance (NMR) spectra were measured at 25 °C on a 400 MHz Bruker AVANCE III AMX system. To obtain the ³¹P NMR spectra, the samples were prepared according to the protocol shown by Balakshin and Capanema.⁴⁴ In this protocol, the hydroxyl groups of lignin are initially completely converted using 2-chloro-4,4,5,5-tetramethyl-1,3,2-dioxaphospholane. Subsequently, the quantification of the converted hydroxyl groups is performed using the phosphorylated endo-*N*-hydroxy-5-norbornene-2,3-dicarboximide as an internal standard.

2.4.2. Fourier Transform Infrared Spectroscopy. Fourier transform infrared (FTIR) spectra of resins and 3D-printed samples were

recorded at room temperature using a Bruker ALPHA spectrometer equipped with an ATR single reflection crystal (Bruker Optic GmbH). Spectra were obtained in the range between 4000 and 400 cm^{-1} (64 scans). Background spectra were recorded against air.

2.4.3. Optical and Atomic Force Microscopy. 3D-printed samples, which had not yet undergone mechanical testing, were fractured at room temperature in a direction perpendicular to the layer additive direction to reveal their bulk surfaces (see Figure S4b in the Supporting Information). Before conducting atomic force microscopy (AFM) imaging on selected spots, the quality of the fractured surfaces was examined by using optical microscopy (OM) (Olympus BX60, Japan). For AFM imaging, a setup consisting of a Multimode and NanoScope V controller AFM (Bruker, USA) was employed with the JV vertical engage scanner. The system was operated in PeakForce Tapping conjugated to quantitative nanomechanical mapping (PF-QNM). Silicon-made cantilevers (nominal spring constant of 2 N m^{-1} , nominal tip apex radius of 9 nm, Olympus, model OMCL-AC240TS) were utilized. The AFM’s optical sensitivity (deflection sensitivity) was determined using the thermal tune method, based on the nominal values of the cantilever’s spring constant.⁴⁵ The measurements were conducted in air at controlled temperatures (21 °C) and with a relative humidity of approximately 40%. In the AFM software (NanoScope, version 9.7), the scanning parameters, such as scan rate, feedback loop, and applied load, were set to “off” to apply specific constant values chosen by the AFM operator. The data were collected following a sine-wave sample-tip trajectory with a frequency of 1–2 kHz and a peak-force amplitude value of 80–150 nm. Data analysis was performed by using the NanoScope Analysis software (version 3.0).

2.4.4. Vis–NIR Spectroscopy. Visible–near-infrared (vis–NIR) absorption spectra were captured for 3D-printed samples in the range of 415–900 nm with a Lambda 850 (PerkinElmer, USA) spectrophotometer. The vis–NIR spectra of 3D-printed polyPEGDA were subtracted from the curves for samples containing methacrylated lignin. Four millimeter thickness samples were used to measure the spectra.

2.4.5. Differential Scanning Calorimetry. The differential scanning calorimetry (DSC) traces for 3D-printed samples (masses of about 5 mg) were recorded through heating–cooling–heating cycles using a DSC 25 from TA Instruments (USA) at a heating/cooling rate of 10 °C min^{-1} in the temperature range between –80 and 40 °C. Glass transition temperature values were determined from the DSC curves as the inflection point of the stepwise change in the endothermic heat flux signal during the first heating run.

2.4.6. Thermogravimetric Analysis. The thermal resistance was investigated with a TGA 550 thermal gravimetric analyzer (TA Instruments, US). Thermogravimetric analysis (TGA) curves were captured for samples (around 9 mg) in Al_2O_3 crucibles from 45 to 590 °C at a heating rate of 10 °C min^{-1} under a nitrogen atmosphere.

2.4.7. Tensile Testing. Static mechanical properties were characterized by tensile testing on standard ASTM-D638 type IV tensile bars with a thickness of 4 mm using an Instron 5565A apparatus at 50 mm min^{-1} crosshead speed with a 5 kN load cell. Values of Young’s modulus (fitting: from 0.2 to 0.8% of the deformation), tensile stress at break, and elongation at break were calculated/measured. Eight samples per each type were tested, and the results were averaged.

2.4.8. DPPH Assay. Samples were studied at room temperature for their antioxidant activity with the 2,2-diphenyl-1-picrylhydrazyl (DPPH) colorimetric assay based on the modified Blois methodology reported by Boarino et al.^{46,47} DPPH is a stable free radical with a purple color which turns yellow when scavenged.⁴⁸ 40 mg-pieces of the 3D-printed tensile bars were shredded and placed in UV–vis cuvettes with 2 mL of a DPPH solution in methanol (25 mg L^{-1}). The aluminum-covered cuvettes (UV light protection) were stirred in the shaker (Knytel, model K-MI0103002) for 3 h. The absorbance of the DPPH solution at the absorption band at 517 nm wavelength was measured by a spectrophotometer (Jasco, model V-630). The percentage of antioxidant activity was calculated as $[(A_{\text{DPPH}} - A_{\text{DPPH-3h}})/A_{\text{DPPH}}] \times 100$, where A_{DPPH} is the absorbance of pure

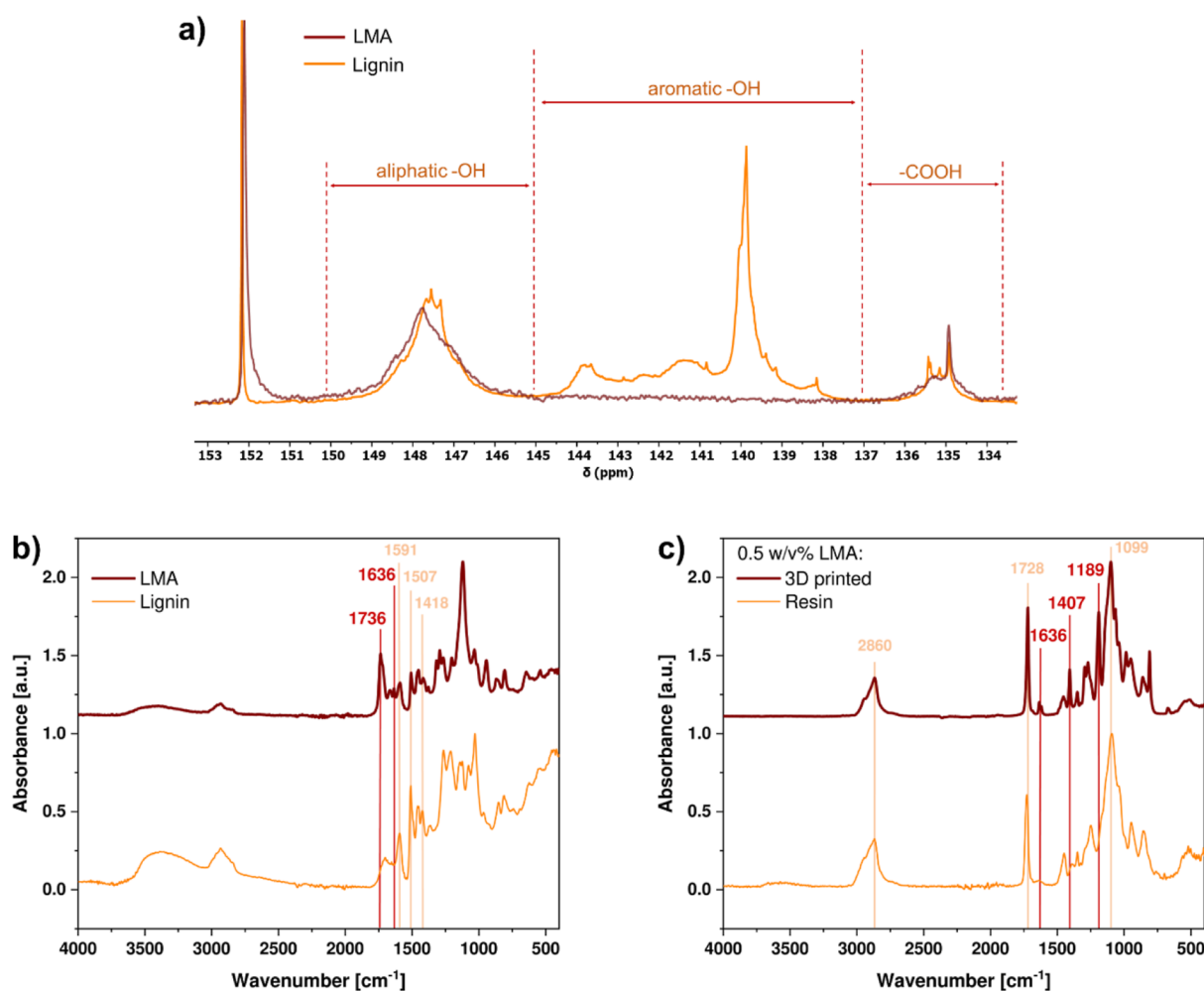


Figure 1. (a) ^{31}P NMR and (b) FT-IR spectra of lignin and methacrylated lignin. For ^{31}P NMR, derivatization with 2-chloro-4,4,5,5-tetramethyl-1,3,2-dioxaphospholane was performed. (c) FT-IR spectra of resin and a 3D-printed sample containing 0.5 w/v % of the methacrylated lignin.

DPPH solution at 517 nm wavelength and $A_{\text{DPPH-3h}}$ is the absorbance of the DPPH solution after 3 h of incubation with shredded samples. The measurement was repeated four times, and the results were averaged.

2.4.9. Statistics. To compare statistically the differences of mean, the analysis of variance (ANOVA statistics in OriginPro 2021b software) using the Tukey test at a significant level of $p < 0.05$ (for an evidence) and $p < 0.1$ (for a trend) was performed for tensile testing and DPPH assay data, respectively.

3. RESULTS AND DISCUSSION

3.1. Copolymerization of Methacrylated Lignin and PEGDA via 3D Printing. The methacrylation of Kraft lignin with methacrylic anhydride was confirmed by both FTIR spectroscopy and derivatization ^{31}P NMR (Figure 1). To perform the NMR analysis, lignin and methacrylated lignin were derivatized with 2-chloro-4,4,5,5-tetramethyl-1,3,2-dioxaphospholane (153 ppm) in the presence of a standard (133 ppm). Resonances that represent aliphatic- and aromatic-OH as well as carboxylic acid are visible in the spectrum (Figure 1a). As ^1H and ^{13}C NMR analyses frequently face the challenge of significant overlap of lines in the spectrum, this derivatization technique using ^{31}P NMR enables the analysis of lignin-based samples, allowing the quantification of hydroxyl and carboxylic acid groups before and after the reaction. The obtained transformations of >99.5% of aromatic hydroxyl

groups were similar to our previous works.^{21,49} In the FTIR spectra of the methacrylated lignin, the vibration bands at 1736 cm^{-1} correspond to the carbonyl ($\text{C}=\text{O}$) of the methacrylate, and the bands at 1636 and 808 cm^{-1} correspond to the carbon-carbon double bond ($\text{C}=\text{C}$) confirming the formation of the methacrylic acid ester (Figure 1b). Furthermore, a substantial reduction in the intensity of the broad band associated with the hydroxyl group ($-\text{OH}$) in the range of 3000–3800 cm^{-1} was observed, indicating the successful esterification of the hydroxyl groups in lignin. The slight spectral differences compared to the literature are attributed to the different sources of lignin.^{21,22} Some lignin characteristic IR absorbance bands can be distinguished at the region comprising 1591, 1507, and 1418 cm^{-1} that correspond to the aromatic skeleton of lignin.⁵⁰

All resin compositions showed miscibility and lack of turbidity (Figure S1 in the Supporting Information), confirmed by no light scattering by green-laser illumination. For FTIR of resin and a 3D-printed sample containing 0.5 w/v % of the methacrylated lignin, the reduction of the bands at 1636 and 1407 cm^{-1} corresponding to the vinyl groups confirms the cross-linking of the PEGDA chains (Figure 1c). Both spectra show the bands at 2860 cm^{-1} corresponding to the $-\text{CH}_2-$ of the chain, 1728 cm^{-1} corresponding to the $\text{C}=\text{O}$ of the acrylate, and 1099 cm^{-1} corresponding to the $-\text{O}-$ of the



Figure 2. Photos of 3D-printed samples encompassed polyPEGDA with methacrylated lignin at the content as indicated: (a) tensile bars; (b) elephant, nanotube, fullerene, and gyroid sphere. The upper inset in (b) is an optical microscopy image that shows the linking of model arms in the fullerene structure for a sample containing 5 w/v % of the methacrylated lignin.

chain. The FTIR spectra for samples with higher lignin concentrations reveal similar spectra (cf. Figure S3a in the Supporting Information for the 5.0 w/v % of the methacrylated lignin). However, the FTIR spectra of the sample with 10.0 w/v % of the methacrylated lignin indicate a lower conversion of the double bonds, e.g., with band intensities at 1407 and 1191 cm^{-1} (Figure S3b in the Supporting Information), thus limited solidification.

We have 3D-printed diverse models with various spatial complexity (Figure 2), quantity (Figure S4a in the Supporting Information), and sizing (Figure S5 in the Supporting Information). Up to 5 w/v % of the methacrylated lignin in PEGDA, all structures were printable and showed remarkable submillimeter detailing. Also, the tensile bars (115 mm in length) exhibited a consistent homogeneous color across their length, which, combined with the long 3D-printing time (about 36 h), indicates stable manufacturing without material phase separation or lignin sedimentation. Optical microscopy

analysis demonstrated proper bonding of layers, free of micrometer-sized defects, e.g., voids (inset in Figures 2b and 3a,b).

Some tensile bars with 7.5 w/v % of the methacrylated lignin were not printed completely. Breaks in 3D prints randomly occur at various points along their lengths (Figure 2a). All samples with 10.0 w/v % of the methacrylated lignin were not 3D-printed as intended; only the bottom layers were printed (Figure 2a). We attribute this issue to a decrease in the efficiency of layer bonding. This is caused by the high absorption of UV light by lignin at this concentration, which not only inhibits photopolymerization but also interferes with lignin's radical scavenging properties.^{4,20,28} High UV light absorption is also confirmed by the UV-vis absorption spectra (Figure 4a).

3.2. Lignin Solubility at Layers and Interfaces of 3D-Printed Samples. The effect of the incorporation of the methacrylated lignin into the polyPEGDA matrix at the

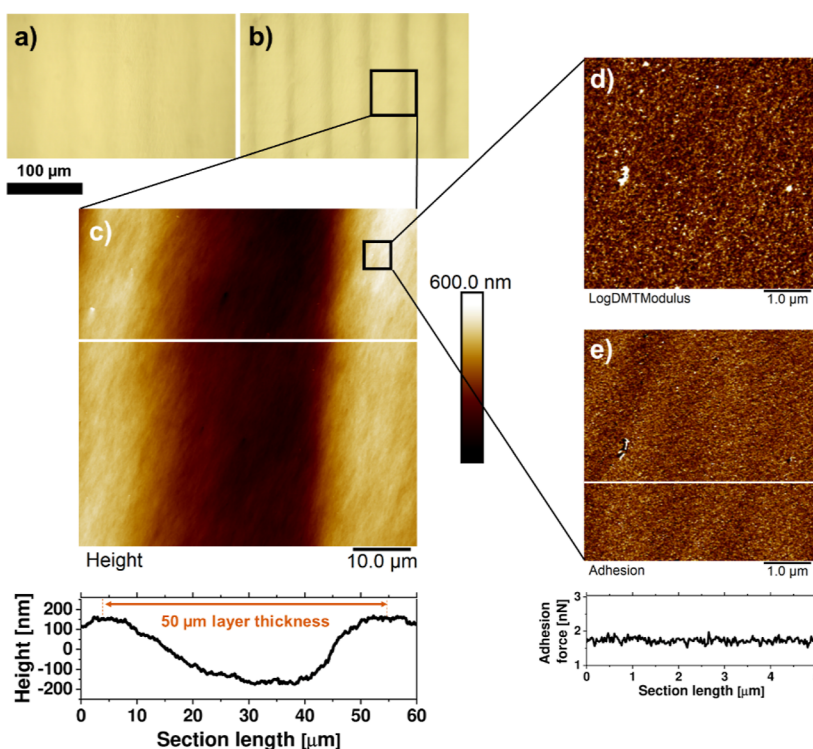


Figure 3. Lignin solubility in polyPEGDA was determined by microscopies. OM data of (a) 3D-printed polyPEGDA and (b) 3D-printed polyPEGDA with methacrylated lignin at 5.0% w/v %. AFM data of polyPEGDA with methacrylated lignin at 5.0% w/v %: (c) height image with a cross-section plot; the orange arrow indicates the borderline between the beginning of layer (n) and layer ($n + 1$), thus layer thickness, (d) Young's modulus map, and (e) adhesion force map with a cross-section plot. Black squares represent zoom-ins.

micrometer and submicrometer scales was analyzed by OM and quantitative AFM observation (Figure 3). The vertical lines in OM images (Figure 3a,b) are associated with interfaces, i.e., areas where consecutive layers are bounded. Each sample shows a topological oscillation in the fractured area that is related to the skewed profile in each individual layer and the presence of the interfaces. This observation is rationalized by a spatial variation of the copolymer cross-linking density as the light absorption varies across the layers (different double bond conversions across the layers and interfaces).^{51,52} The greater the methacrylated lignin content, the more significant the variation in the surface profile across the layers (as shown in Figure 3c and the cross-section plot). The analysis of the $60 \times 60 \mu\text{m}^2$ surface area indicated neither aggregates nor agglomerates of the methacrylated lignin in the polyPEGDA matrix. Moreover, high-resolution mapping of both the AFM Young's modulus (Figure 3d) and adhesion force (Figure 3e) indicates the homogeneous morphology of the samples. Both maps exhibit low data contrast, indicating high solubility of the methacrylated lignin in the polyPEGDA matrix. This implies successful statistical copolymerization during photopolymerization.

3.3. Characterization of 3D-Printed Lignin-PolyPEGDA Copolymers.

3.3.1. Optical Properties. An intrinsic property of lignin is its UV-vis absorption due to its aromatic nature, making materials containing lignin an interesting choice as a biobased, broad-spectrum light blocker.^{20,53} Thus, even small amounts of lignin in the copolymer can be appreciated visually and quantitatively (Figures 2 and 4a). In Figure 4a, we present data above 415 nm of the wavelength and up to an absorbance of 3, as these are thresholds for a reliable spectrophotometer sensitivity (0.1% of the light trans-

mittance). We selected the wavelength of 550 nm to be a reference for the spectra comparison. Already at 0.5 and 1 w/v % lignin content, the samples' light transmittance was reduced significantly to ca. 30–35% compared to air. For higher lignin loading, light transmittance is even further reduced to be 11, 4, 1, and 0.1% for samples with 2, 3, 5, and 7.5 w/v % lignin content, respectively. Importantly, these low amounts of lignin are sufficient to completely block the UV-A, UV-B, and UV-C spectra in the samples we studied (thickness of 4 mm).^{54,55} As the PEGDA and polyPEGDA (Figure S6 in the Supporting Information) are barely absorbing light in the UV-B–NIR spectrum, the lignin content also improves the VIS-shielding properties of the manufactured samples.^{56,57}

3.3.2. Thermal Properties. The presence of lignin in the copolymers has only a minor impact on the T_g . Rather, no change is observed up to 5% (w/v) of the lignin content (from -23 to -27 °C, Figure 4b). However, a stable T_g is a key point for lignin-based compositions to be used, for instance, as hydrogels or cryogels.^{58–60} At higher lignin contents, i.e., 7.5–10.0 w/v %, the T_g decreased to lower temperatures. Most likely, the presence of lignin, as the amorphous polymer, increases the chain mobility in the polymer matrix and thus reduces the T_g . Dried Kraft lignin typically exhibits T_g between 100 and 170 °C.⁶¹ Therefore, one would expect an opposite trend in our DSC traces, even when considering the potential impact of absorbed water on lignin, which could reduce its T_g (e.g., relative humidity ca. 45% can reduce lignin's T_g by a factor of 2).⁶²

The complex chemical structure of lignin, especially phenylpropane units and ether linkages, contributes to its resistance to heat-induced degradation.⁶³ The main weight loss of the methacrylated lignin is in the broad range of 300–500

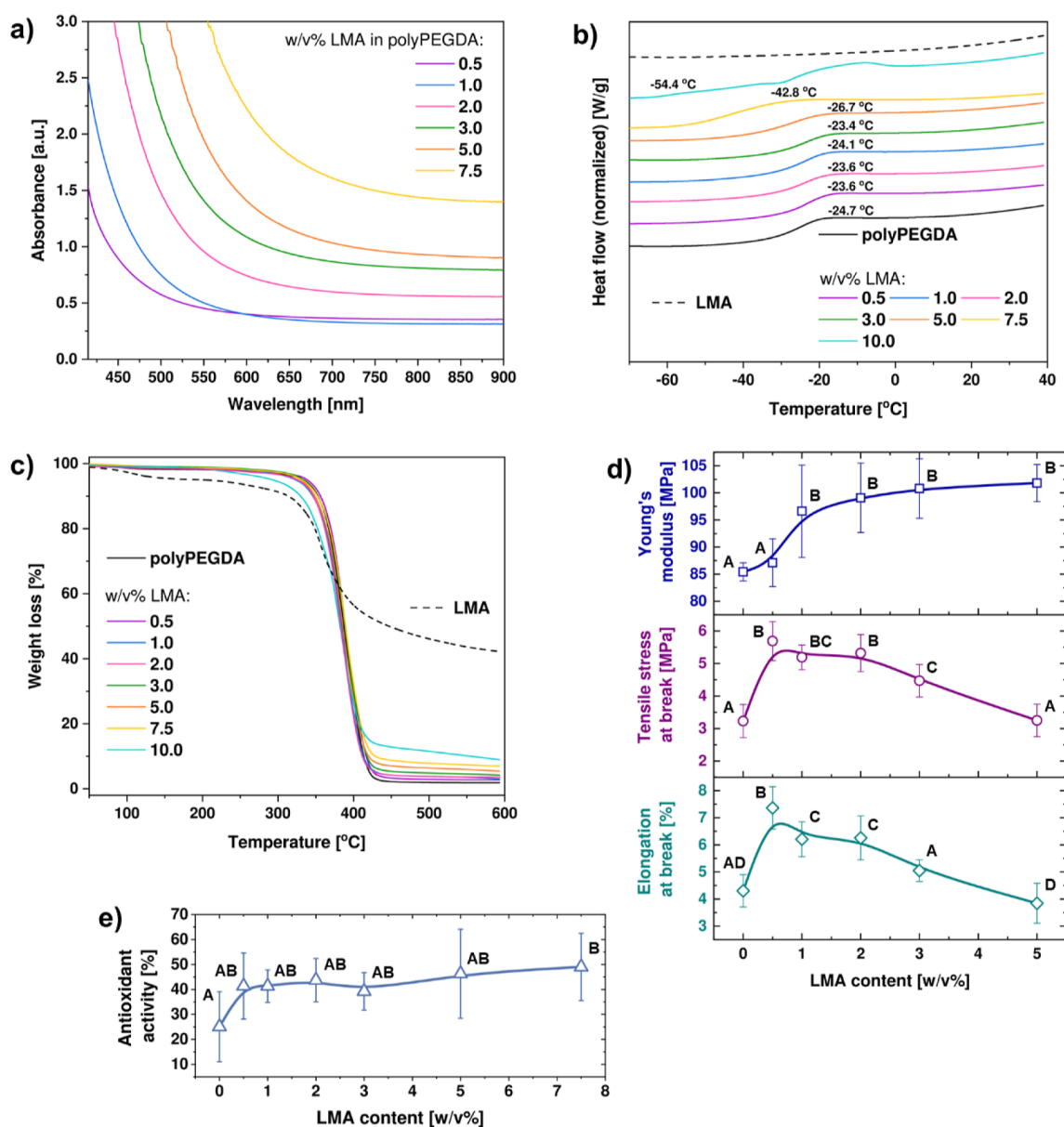


Figure 4. Characterization of lignin-PEGDA copolymers: (a) vis absorption spectra; the spectra of 3D-printed polyPEGDA were subtracted from the curves, (b) DSC traces; glass transition temperature is indicated, (c) TGA curves, (d) calculated/measured results of tensile testing: Young's modulus, tensile stress at break, and elongation at break, (e) calculated results of antioxidant activity. In (d,e), curves are guides to eyes, error bars represent standard deviation, and capital letters indicate results of the Tukey analysis (means that do not share a letter are significantly different).

°C temperature (Figure 4c). Similar results were obtained by Yiamsawas et al.²² The amount of char residue content at 500 °C for 3D-printed samples increases from 1.9, through 6.4, to 11.5% for polyPEGDA with the methacrylated lignin at 0, 5.0, and 10.0 w/v % loading.

3.3.3. Mechanical Properties. Kraft lignin contains a high portion of rigid aromatic units, which not only impart thermal stability but also contribute to the stiffness of materials.^{64,65} A mechanical reinforcement is visible for Young's modulus values at elevated loading of the methacrylated lignin, e.g., up to 15–20% higher stiffness at 5.0 w/v % loading (Figure 4d). The incorporation of the methacrylated lignin also resulted in a noticeable increase of elongation at break, e.g., higher by a factor of 1.7 at only 0.5 w/v % loading. This conclusion is reflected in the statistical analysis by the Tukey test, which confirms that there is a difference between the group's means

(in Figure 4d, means that do not share A, B, or C letters are significantly different). The greater variability in Young's modulus data is attributed to the necessity of employing a functional fit to the experimental points. Unlike the results of tensile stress and elongation at breaks, the fit is an additional source of error. Considering the data of the elongation at break, one could state that our 3D-printed samples work like a mechanical absorber and dissipate mechanical energy. Thus, lignin improves the resistance and fracture toughness of the copolymers studied.^{4,61,62} This property is limited beyond 5.0 w/v % loading, probably because of the higher cross-linking density that is also visible in the high tensile Young's modulus value. Given that polyPEGDA, unlike other elastomers, is a highly brittle polymer with a low value of Young's modulus, the mechanical "optimum" can be found for a composition with a 2.0 w/v % content of the methacrylated lignin. For this

loading, all three parameters, i.e., Young's modulus, tensile stress at break, and elongation at break have relatively the highest values.

3.3.4. Antioxidant Properties. Lignin's antioxidant properties are another intrinsic benefit for lignin being used as an additive or a comonomer.^{2,18} We studied the antioxidant properties of the 3D-printed copolymers by a typical DPPH assay.^{46,47} The absorbance of the DPPH solution was measured at 517 nm, which was significantly decreased in the presence of the 3D-printed samples (cf. Figure S7). This reduction of absorbance quantifies the reduction of the stable free-radical species of DPPH, which decreases the color of the mixture. The reduction of absorbance corresponds to the antioxidant activity of the samples (Figure 4e). 3D-printed (neat) polyPEGDA exhibited moderate antioxidant activity which might be attributed to residual vinyl groups and photoinitiators. For the 3D-printed specimen containing our lignin-PEGDA copolymers, already 0.5 w/v % lignin content resulted in an increase of up to 40% of the antioxidant activity. At higher loadings, this value increases to approximately 50%, but the content of the methacrylated lignin with the resulting antioxidant properties does not scale significantly and rather undergoes a plateau. The uncertainty of this measurement is related to the way the samples are shredded (the surface area of the pieces in contact with the DPPH solution and their quantity) and is visible in the error bars. However, the Tukey test confirms a visible trend in the antioxidant activity related to the presence of lignin in the 3D-printed polyPEGDA samples.

Because we are the first to present the results of the antioxidant activity of a lignin-containing copolymer obtained via vat 3D photopolymer printing, these results can be compared only to those of other systems. For instance, Boarino et al. showed that for poly(lactic acid)-grafted lignin nanoparticles, at 1 wt % lignin content, the antioxidant activity of 40% can be obtained.⁴⁷ Although there is no universally fixed minimum value of the antioxidant activity (determination is based on the specific requirements), this level is enough for the material to help trap and neutralize free radicals in the medium in which it is placed.⁶⁶

Our results indicate that the tested material can be used to 3D print objects that provide a barrier to oxidation. As the antioxidant activity (percentage) depends on the concentration of the incubated samples and the time of their incubation, the antioxidant activity of our system can be further controlled and adjusted.^{48,67} Therefore, our samples may exhibit comparable radical scavenging abilities to commercial ones.⁶⁶

4. SUMMARY AND CONCLUSIONS

We conducted a study on 3D-printed materials produced through the photopolymerization of synthetic PEGDA and biobased methacrylated Kraft lignin at varying loadings, up to 10 w/v %. PEGDA and lignin copolymerized with each other. Several methods and techniques were employed, i.e., spectroscopies (NMR, FT-IR, and vis-NIR), microscopies (OM and AFM), thermo- and mechanoanalytical tools (DSC, TGA, and tensile testing), as well as a stable free radical assay to unveil the antioxidant properties of samples.

We have demonstrated that it is possible to create objects of various complexities and sizes using Kraft lignin-based materials with a 3D printer equipped with a single low-intensity UV light source. In contrast to the literature, where only up to 2 wt % of the Kraft lignin could be used for

manufacturing 3D-printed photopolymers,^{28,29} we reached the threshold of 5 w/v % for fully 3D-printed objects. As can be inferred from data obtained for samples with lignin content exceeding 5 w/v %, the loading limit can be further extended when a 3D printer with higher light exposure or more light sources is employed for additive manufacturing. Nonetheless, in cases where a substantial portion of lignin cannot be used for the resin composition, recent research indicates that PEG can also be derived from renewable sources (and probably diacrylated to PEGDA).^{68,69} Then, the resin composed of both would essentially be a fossil-free material. Recent reports also suggest that lignin could be a material suitable for biomedical applications.¹⁶ This feature would enhance the synergy between polyPEGDA and lignin in biomaterial applications such as tissue engineering.

Thoroughly dissolved methacrylated lignin was confirmed by OM and quantitative AFM visualization of the bulk surface (fractured). Unlike others, our resin is well-defined chemically, and it forms a statistical copolymer.

Particles limit the layer thickness to be set for 3D printing and weaken the interfaces by deforming them. When using our resin, the layer thickness can be reduced upon request, for example, to 10 μm (if supported by the 3D printer), thus offering improved resolution in additive manufacturing. Furthermore, the decreased layer thickness allows for more effective resin curing by light (as the absorption path is shorter). Therefore, it should be possible to use a higher loading of Kraft lignin-based content with low-power 3D printers as well.

Our study demonstrates that increased properties of commodity polymers by lignin additives in low amounts are possible. This could lead to a decrease in the utilization of petroleum-based polymers. Although this was not the focus of interest in our article, our system also has a potential capability for accelerated biodegradation as the lignin is a biodegradable biopolymer.^{2,5} We have also noted that our resin compositions remain stable (no sedimentation and no phase separation) for an extended period (>6 months). Therefore, it holds promise for potential commercialization.

In conclusion, our research paves the way for future investigations by exploring the potential of utilizing photopolymer 3D printing and PEGDA and lignin-based materials to create functional materials with specific properties. This presents exciting possibilities, including the development of light-blocking hydrogel scaffolds to shield against sun radiation and the creation of structurally diverse objects with controlled oxidation. These findings provide a foundation for obtaining interesting materials with unique architectures and functionalities.

■ ASSOCIATED CONTENT

Supporting Information

The Supporting Information is available free of charge at <https://pubs.acs.org/doi/10.1021/acsapm.3c01875>.

Photos of liquid prepolymer formulations, ETC tool procedure, FT-IR spectra of resin and 3D-printed samples, photos and images of printed samples, UV-vis absorption spectra of 3D-printed polyPEGDA sample, and UV-vis absorption spectra (antioxidation activity) of lignin-containing 3D-printed samples (PDF)

AUTHOR INFORMATION

Corresponding Author

Hubert Gojzewski – Sustainable Polymer Chemistry,
Department of Molecules & Materials, Faculty of Science and
Technology, University of Twente, MESA+ Institute for
Nanotechnology, 7522 NB Enschede, The Netherlands;
orcid.org/0000-0001-6325-8293; Email: h.gojzewski@
utwente.nl

Authors

Ana Laura Ruiz Deance – Sustainable Polymer Chemistry,
Department of Molecules & Materials, Faculty of Science and
Technology, University of Twente, MESA+ Institute for
Nanotechnology, 7522 NB Enschede, The Netherlands

Bjorn Siersema – Sustainable Polymer Chemistry,
Department of Molecules & Materials, Faculty of Science and
Technology, University of Twente, MESA+ Institute for
Nanotechnology, 7522 NB Enschede, The Netherlands

Laurine Eleonora Anne-Catherine Yoe – Sustainable
Polymer Chemistry, Department of Molecules & Materials,
Faculty of Science and Technology, University of Twente,
MESA+ Institute for Nanotechnology, 7522 NB Enschede,
The Netherlands

Frederik R. Wurm – Sustainable Polymer Chemistry,
Department of Molecules & Materials, Faculty of Science and
Technology, University of Twente, MESA+ Institute for
Nanotechnology, 7522 NB Enschede, The Netherlands;
orcid.org/0000-0002-6955-8489

Complete contact information is available at:
<https://pubs.acs.org/10.1021/acsapm.3c01875>

Notes

The authors declare no competing financial interest.

ACKNOWLEDGMENTS

We acknowledge Clemens Padberg (UT) and Ramon ten Elshof (UT) for help with some experiments and characterizations. We acknowledge Qisong Hu (UT) for help with the NMR calculations. We also acknowledge Stefan Peil and Prof. Dr. Ian Gibson for valuable discussions.

REFERENCES

- (1) Vinod, A.; Sanjay, M. R.; Suchart, S.; Jyotishkumar, P. Renewable and sustainable biobased materials: An assessment on biofibers, biofilms, biopolymers and biocomposites. *J. Clean Prod.* **2020**, *258*, 120978.
- (2) Kai, D.; Tan, M. J.; Chee, P. L.; Chua, Y. K.; Yap, Y. L.; Loh, X. J. Towards lignin-based functional materials in a sustainable world. *Green Chem.* **2016**, *18* (5), 1175–1200.
- (3) Singh, A.; Christensen, T.; Panoutsou, C. Policy review for biomass value chains in the European bioeconomy. *Glob. Transit.* **2021**, *3*, 13–42.
- (4) Jiang, B.; Jiao, H.; Guo, X.; Chen, G.; Guo, J.; Wu, W.; Jin, Y.; Cao, G.; Liang, Z. Lignin-Based Materials for Additive Manufacturing: Chemistry, Processing, Structures, Properties, and Applications. *Adv. Sci.* **2023**, *10* (9), 2206055.
- (5) Tardy, B. L.; Lizundia, E.; Guizani, C.; Hakkarainen, M.; Sipponen, M. H. Prospects for the integration of lignin materials into the circular economy. *Mater. Today* **2023**, *65*, 122–132.
- (6) Figueiredo, P.; Lintinen, K.; Hirvonen, J. T.; Kostianen, M. A.; Santos, H. A. Properties and chemical modifications of lignin: Towards lignin-based nanomaterials for biomedical applications. *Prog. Mater. Sci.* **2018**, *93*, 233–269.
- (7) Schutyser, W.; Renders, T.; Van Den Bosch, S.; Koelewijn, S. F.; Beckham, G. T.; Sels, B. F. Chemicals from lignin: An interplay of lignocellulose fractionation, depolymerisation, and upgrading. *Chem. Soc. Rev.* **2018**, *47* (3), 852–908.
- (8) Jacobs, B.; Yao, Y.; Van Nieuwenhove, I.; Sharma, D.; Graulus, G. J.; Bernaerts, K.; Verberckmoes, A. Sustainable lignin modifications and processing methods: green chemistry as the way forward. *Green Chem.* **2023**, *25* (6), 2042–2086.
- (9) Carvajal, J. C.; Gómez, Á.; Cardona, C. A. Comparison of lignin extraction processes: Economic and environmental assessment. *Bioresour. Technol.* **2016**, *214*, 468–476.
- (10) Wu, J.; Liu, Q.; Wang, C.; Wu, W.; Han, W. Investigation of lignin as an alternative extender of bitumen for asphalt pavements. *J. Clean Prod.* **2021**, *283*, 124663.
- (11) Yuliestyan, A.; García-Morales, M.; Moreno, E.; Carrera, V.; Partal, P. Assessment of modified lignin cationic emulsifier for bitumen emulsions used in road paving. *Mater. Des.* **2017**, *131*, 242–251.
- (12) Pérez, I. P.; Rodríguez Pasandín, A. M.; Pais, J. C.; Alves Pereira, P. A. Use of lignin biopolymer from industrial waste as bitumen extender for asphalt mixtures. *J. Clean Prod.* **2019**, *220*, 87–98.
- (13) Sekar, P.; Noordermeer, J. W. M.; Anyszka, R.; Gojzewski, H.; Podschun, J.; Blume, A. Hydrothermally Treated Lignin as a Sustainable Biobased Filler for Rubber Compounds. *ACS Appl. Polym. Mater.* **2023**, *5* (4), 2501–2512.
- (14) Kun, D.; Pukánszky, B. Polymer/lignin blends: Interactions, properties, applications. *Eur. Polym. J.* **2017**, *93*, 618–641.
- (15) Gordobil, O.; Herrera, R.; Yahyaoui, M.; İlk, S.; Kaya, M.; Labidi, J. Potential use of kraft and organosolv lignins as a natural additive for healthcare products. *RSC Adv.* **2018**, *8* (43), 24525–24533.
- (16) Sugiarto, S.; Leow, Y.; Tan, C. L.; Wang, G.; Kai, D. How far is Lignin from being a biomedical material? *Bioact. Mater.* **2022**, *8*, 71–94.
- (17) Machado, T. O.; Grabow, J.; Sayer, C.; de Araújo, P. H.; Ehrenhard, M. L.; Wurm, F. R. Biopolymer-based nanocarriers for sustained release of agrochemicals: A review on materials and social science perspectives for a sustainable future of agri- and horticulture. *Adv. Colloid Interface Sci.* **2022**, *303*, 102645.
- (18) Yearla, S. R.; Padmasree, K. Preparation and characterisation of lignin nanoparticles: evaluation of their potential as antioxidants and UV protectants. *J. Exp. Nanosci.* **2016**, *11* (4), 289–302.
- (19) Liao, J. J.; Latif, N. H. A.; Trache, D.; Brosse, N.; Hussin, M. H. Current advancement on the isolation, characterization and application of lignin. *Int. J. Biol. Macromol.* **2020**, *162*, 985–1024.
- (20) Zhang, Y.; Naebe, M. Lignin: A Review on Structure, Properties, and Applications as a Light-Colored UV Absorber. *ACS Sustain. Chem. Eng.* **2021**, *9* (4), 1427–1442.
- (21) Fischer, J.; Beckers, S. J.; Yiamsawas, D.; Thines, E.; Landfester, K.; Wurm, F. R. Targeted Drug Delivery in Plants: Enzyme-Responsive Lignin Nanocarriers for the Curative Treatment of the Worldwide Grapevine Trunk Disease Esca. *Adv. Sci.* **2019**, *6* (15), 1802315.
- (22) Yiamsawas, D.; Beckers, S. J.; Lu, H.; Landfester, K.; Wurm, F. R. Morphology-Controlled Synthesis of Lignin Nanocarriers for Drug Delivery and Carbon Materials. *ACS Biomater. Sci. Eng.* **2017**, *3* (10), 2375–2383.
- (23) Liu, X.; Yin, H.; Zhang, Z.; Diao, B.; Li, J. Functionalization of lignin through ATRP grafting of poly(2-dimethylaminoethyl methacrylate) for gene delivery. *Colloids Surf., B* **2015**, *125*, 230–237.
- (24) Ebers, L. S.; Arya, A.; Bowland, C. C.; Glasser, W. G.; Chmely, S. C.; Naskar, A. K.; Laborie, M. P. 3D printing of lignin: Challenges, opportunities and roads onward. *Biopolymers* **2021**, *112* (6), No. e23431.
- (25) Gibson, I.; Rosen, D.; Stucker, B.; Khorasani, M. *Additive Manufacturing Technologies*; Springer International Publishing, 2021.
- (26) Ngo, T. D.; Kashani, A.; Imbalzano, G.; Nguyen, K. T. Q.; Hui, D. Additive manufacturing (3D printing): A review of materials,

- methods, applications and challenges. *Composites, Part B* **2018**, *143*, 172–196.
- (27) Nguyen, N. A.; Bowland, C. C.; Naskar, A. K. A general method to improve 3D-printability and inter-layer adhesion in lignin-based composites. *Appl. Mater. Today* **2018**, *12*, 138–152.
- (28) Zhang, S.; Li, M.; Hao, N.; Ragauskas, A. J. Stereolithography 3D Printing of Lignin-Reinforced Composites with Enhanced Mechanical Properties. *ACS Omega* **2019**, *4* (23), 20197–20204.
- (29) Yao, J.; Morsali, M.; Moreno, A.; Sipponen, M. H.; Hakkarainen, M. Lignin nanoparticle-enhanced biobased resins for digital light processing 3D printing: Towards high resolution and tunable mechanical properties. *Eur. Polym. J.* **2023**, *194*, 112146.
- (30) Johnson, R. M.; Cortés-Guzmán, K. P.; Perera, S. D.; Parikh, A. R.; Ganesh, V.; Voit, W. E.; Smaldone, R. A. Lignin-based covalent adaptable network resins for digital light projection 3D printing. *J. Polym. Sci.* **2023**, *1*, 20230026.
- (31) Zhang, X.; Keck, S.; Qi, Y.; Baudis, S.; Zhao, Y. Study on Modified Dealkaline Lignin as Visible Light Macromolecular Photoinitiator for 3D Printing. *ACS Sustain. Chem. Eng.* **2020**, *8* (29), 10959–10970.
- (32) Sutton, J. T.; Rajan, K.; Harper, D. P.; Chmely, S. C. Lignin-Containing Photoactive Resins for 3D Printing by Stereolithography. *ACS Appl. Mater. Interfaces* **2018**, *10* (42), 36456–36463.
- (33) Feng, X.; Yang, Z.; Chmely, S.; Wang, Q.; Wang, S.; Xie, Y. Lignin-coated cellulose nanocrystal filled methacrylate composites prepared via 3D stereolithography printing: Mechanical reinforcement and thermal stabilization. *Carbohydr. Polym.* **2017**, *169*, 272–281.
- (34) Feng, X.; Yang, Z.; Wang, S.; Wu, Z. The reinforcing effect of lignin-containing cellulose nanofibrils in the methacrylate composites produced by stereolithography. *Polym. Eng. Sci.* **2022**, *62* (9), 2968–2976.
- (35) Keck, S.; Liske, O.; Seidler, K.; Steyrer, B.; Gorsche, C.; Knaus, S.; Baudis, S. Synthesis of a Liquid Lignin-Based Methacrylate Resin and Its Application in 3D Printing without Any Reactive Diluents. *Biomacromolecules* **2023**, *24* (4), 1751–1762.
- (36) Sutton, J. T.; Rajan, K.; Harper, D. P.; Chmely, S. C. Improving uv curing in organosolv lignin-containing photopolymers for stereolithography by reduction and acylation. *Polymers* **2021**, *13* (20), 3473.
- (37) Ibrahim, F.; Mohan, D.; Sajab, M. S.; Bakarudin, S. B.; Kaco, H. Evaluation of the compatibility of organosolv lignin-graphene nanoplatelets with photo-curable polyurethane in stereolithography 3D printing. *Polymers* **2019**, *11* (10), 1544.
- (38) Choi, J. R.; Yong, K. W.; Choi, J. Y.; Cowie, A. C. Recent advances in photo-crosslinkable hydrogels for biomedical applications. *BioTechniques* **2019**, *66* (1), 40–53.
- (39) Morris, V. B.; Nimbalkar, S.; Younesi, M.; McClellan, P.; Akkus, O. Mechanical Properties, Cytocompatibility and Manufacturability of Chitosan:PEGDA Hybrid-Gel Scaffolds by Stereolithography. *Ann. Biomed. Eng.* **2017**, *45* (1), 286–296.
- (40) Hakim Khalili, M.; Zhang, R.; Wilson, S.; Goel, S.; Impey, S. A.; Aria, A. I. Additive Manufacturing and Physicomechanical Characteristics of PEGDA Hydrogels: Recent Advances and Perspective for Tissue Engineering. *Polymers* **2023**, *15* (10), 2341.
- (41) Zhu, J. Bioactive modification of poly(ethylene glycol) hydrogels for tissue engineering. *Biomaterials* **2010**, *31* (17), 4639–4656.
- (42) Gojzewski, H.; Sadej, M.; Andrzejewska, E.; Kokowska, M. Dataset for acrylate/silica nanoparticles formulations and photocured composites: Viscosity, filler dispersion and bulk Poisson's ratio. *Data Brief* **2017**, *12*, 528–534.
- (43) Jacobs, P. F.; Reid, D. T. *Rapid Prototyping & Manufacturing: Fundamentals of Stereolithography*; Society of Manufacturing Engineers, 1992.
- (44) Balakshin, M.; Capanema, E. On the quantification of lignin hydroxyl groups with ³¹P and ¹³C NMR spectroscopy. *J. Wood Chem. Technol.* **2015**, *35* (3), 220–237.
- (45) Hutter, J. L.; Bechhoefer, J. Calibration of atomic-force microscope tips. *Rev. Sci. Instrum.* **1993**, *64*, 1868–1873.
- (46) Blois, M. S. Antioxidant determinations by the use of a stable free radical. *Nature* **1958**, *181* (4617), 1199–1200.
- (47) Boarino, A.; Schreier, A.; Leterrier, Y.; Klok, H. A. Uniformly Dispersed Poly(lactic acid)-Grafted Lignin Nanoparticles Enhance Antioxidant Activity and UV-Barrier Properties of Poly(lactic acid) Packaging Films. *ACS Appl. Polym. Mater.* **2022**, *4* (7), 4808–4817.
- (48) Dawidowicz, A. L.; Wianowska, D.; Olszowy, M. On practical problems in estimation of antioxidant activity of compounds by DPPH method (Problems in estimation of antioxidant activity). *Food Chem.* **2012**, *131* (3), 1037–1043.
- (49) Beckers, S.; Peil, S.; Wurm, F. R. Pesticide-Loaded Nanocarriers from Lignin Sulfonates-A Promising Tool for Sustainable Plant Protection. *ACS Sustain. Chem. Eng.* **2020**, *8* (50), 18468–18475.
- (50) Boeriu, C. G.; Bravo, D.; Gosselink, R. J. A.; Van Dam, J. E. G. Characterisation of structure-dependent functional properties of lignin with infrared spectroscopy. *Ind. Crops Prod.* **2004**, *20* (2), 205–218.
- (51) Gojzewski, H.; Guo, Z.; Grzelachowska, W.; Ridwan, M. G.; Hempenius, M. A.; Grijpma, D. W.; Vancso, G. J. Layer-by-Layer Printing of Photopolymers in 3D: How Weak is the Interface? *ACS Appl. Mater. Interfaces* **2020**, *12* (7), 8908–8914.
- (52) Robakowska, M.; Gibson, I.; Akkerman, R.; Wurm, F. R.; Gojzewski, H. Towards more homogeneous character in 3D printed photopolymers by the addition of nanofillers. *Polym. Test.* **2023**, *129*, 108243.
- (53) Qian, Y.; Qiu, X.; Zhu, S. Lignin: A nature-inspired sun blocker for broadspectrum Sunscreens. *Green Chem.* **2015**, *17* (1), 320–324.
- (54) Skulcova, A.; Majova, V.; Kohutova, M.; Grosik, M.; Sima, J.; Jablonsky, M. UV/Vis Spectrometry as a quantification tool for lignin solubilized in deep eutectic solvents. *BioResources* **2017**, *12* (3), 6713–6722.
- (55) Sadeghifar, H.; Ragauskas, A. Lignin as a UV Light blocker-a review. *Polymers* **2020**, *12* (5), 1134.
- (56) Pelras, T.; Glass, S.; Scherzer, T.; Elsner, C.; Schulze, A.; Abel, B. Transparent low molecularweight poly(ethylene glycol) diacrylate-based hydrogels as film media for photoswitchable drugs. *Polymers* **2017**, *9* (12), 639.
- (57) Lasagni, A.; Yuan, D.; Shao, P.; Das, S. Rapid fabrication of biocompatible hydrogels microdevices using laser interference lithography. *Proc. SPIE-Int. Soc. Opt. Eng.* **2009**, 7365, 73650L.
- (58) Larrañeta, E.; Imízcoz, M.; Toh, J. X.; Irwin, N. J.; Ripolin, A.; Perminova, A.; Domínguez-Robles, J.; Rodríguez, A.; Donnelly, R. F. Synthesis and Characterization of Lignin Hydrogels for Potential Applications as Drug Eluting Antimicrobial Coatings for Medical Materials. *ACS Sustain. Chem. Eng.* **2018**, *6* (7), 9037–9046.
- (59) Madaghiale, M.; Salvatore, L.; Demitri, C.; Sannino, A. Fast synthesis of poly(ethylene glycol) diacrylate cryogels via UV irradiation. *Mater. Lett.* **2018**, *218*, 305–308.
- (60) Meng, Y.; Lu, J.; Cheng, Y.; Li, Q.; Wang, H. Lignin-based hydrogels: A review of preparation, properties, and application. *Int. J. Biol. Macromol.* **2019**, *135*, 1006–1019.
- (61) Wang, C.; Kelley, S. S.; Venditti, R. A. Lignin-Based Thermoplastic Materials. *ChemSusChem* **2016**, *9* (8), 770–783.
- (62) Bouajila, J.; Dole, P.; Joly, C.; Limare, A. Some laws of a lignin plasticization. *J. Appl. Polym. Sci.* **2006**, *102* (2), 1445–1451.
- (63) Brodin, I.; Sjöholm, E.; Gellerstedt, G. The behavior of kraft lignin during thermal treatment. *J. Anal. Appl. Pyrol.* **2010**, *87* (1), 70–77.
- (64) Mimini, V.; Sykacek, E.; Syed Hashim, S. N. A.; Holzweber, J.; Hettegger, H.; Fackler, K.; Potthast, A.; Mundigler, N.; Rosenau, T. Compatibility of Kraft Lignin, Organosolv Lignin and Lignosulfonate With PLA in 3D Printing. *J. Wood Chem. Technol.* **2019**, *39* (1), 14–30.
- (65) Huang, C.; He, J.; Narron, R.; Wang, Y.; Yong, Q. Characterization of Kraft Lignin Fractions Obtained by Sequential Ultrafiltration and Their Potential Application as a Biobased Component in Blends with Polyethylene. *ACS Sustain. Chem. Eng.* **2017**, *5* (12), 11770–11779.

(66) Lu, X.; Gu, X.; Shi, Y. A review on lignin antioxidants: Their sources, isolations, antioxidant activities and various applications. *Int. J. Biol. Macromol.* **2022**, *210*, 716–741.

(67) Zhang, W.; Zeng, Z.; Wei, J. Electrochemical Study of DPPH Radical Scavenging for Evaluating the Antioxidant Capacity of Carbon Nanodots. *J. Phys. Chem. C* **2017**, *121* (34), 18635–18642.

(68) Himmelmann, R.; Otterstaetter, R.; Franke, O.; Brand, S.; Wachsen, O.; Mestl, G.; Effenberger, F.; Klemm, E. Selective oxidation of ethanol to ethylene oxide with a dual-layer concept. *Catal. Commun.* **2022**, *167*, 106424.

(69) Faveere, W. H.; Van Praet, S.; Vermeeren, B.; Dumoleijn, K. N. R.; Moonen, K.; Taarning, E.; Sels, B. F. Toward Replacing Ethylene Oxide in a Sustainable World: Glycolaldehyde as a Bio-Based C2 Platform Molecule. *Angew. Chem., Int. Ed.* **2021**, *60* (22), 12204–12223.